THE JOURNAL OF PHYSICAL CHEMISTRY B

Article

pubs.acs.org/JPCB

Excitation Energy Transfer in the Peridinin-Chlorophyll *a*-Protein Complex Modeled Using Configuration Interaction

William P. Bricker and Cynthia S. Lo*

Department of Energy, Environmental and Chemical Engineering, Washington University, Saint Louis, Missouri 63130, United States

ABSTRACT: We modeled excitation energy transfer (EET) in the peridinin-chlorophyll *a*-protein (PCP) complex of dinoflagellate *Amphidinium carterae* to determine which pathways contribute dominantly to the high efficiency of this process. We used complete active space configuration interaction (CAS-CI) to calculate electronic structure properties of the peridinin (PID) and chlorophyll *a* (CLA) pigments in PCP and the transition density cube (TDC) method to calculate Coulombic couplings between energy transfer donors and acceptors. Our calculations show that the $S_1 \rightarrow Q_y$ EET pathway from peridinin to chlorophyll *a* is the dominant energy transfer pathway in PCP, with two sets of interactions—between PID612 and CLA601 and between PID622 and CLA602—contributing most strongly. EET lifetimes for these two interactions were calculated to be 2.66 and 2.90, with quantum efficiencies of 85.75 and 84.65%, respectively. The calculated Coulombic couplings for EET between two peridinin molecules in the strongly allowed S_2 excited states are extremely large and suggest excitonic coupling between pairs of peridinin S_2 states. This methodology is also broadly applicable to the study of EET in other photosynthetic complexes and/or organic photovoltaics, where both single and double excitations are present and donor and acceptor molecules are tightly packed.

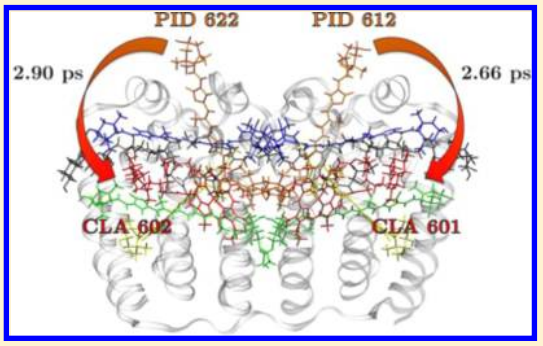

INTRODUCTION

The study of solar energy utilization in photosynthetic organisms, including light harvesting and energy transfer, may give us clues as to how to better capture and store energy in bioinspired or artificial photosynthetic systems. Naturally, there are differences in how photosynthetic organisms behave compared to photovoltaic systems; the organisms' main concern is to utilize sunlight to store energy in the form of chemical bonds, not necessarily to convert all available energy to electrical power output, given appropriate thermodynamic limitations.[1,2] As such, photosynthetic organisms, such as algae, exhibit incredibly high (near 100%) quantum efficiencies in excitation energy transfer, and we seek to better understand the underlying origins of these processes.

We choose as our model the peridinin-chlorophyll *a*-protein (PCP) complex, which is commonly found in dinoflagellates. The structure of PCP in dinoflagellate *Amphidinium carterae* has been successfully determined using X-ray crystallography,[3] as shown in Figure 1.[4−6] PCP is a protein trimer, with eight peridinin (PID) carotenoids and two chlorophyll *a* (CLA) pigments per protein monomer (Figure 2). Peridinin contains a polyene backbone, which is broken up by a lactone ring and an allene group (Figure 2). Thus, energy transfer between similar pigments (i.e., peridinin to peridinin) and dissimilar pigments (i.e., peridinin to chlorophyll *a*) may be investigated in this complex.

The PCP complex in *Amphidinium carterae* has attracted attention from both experimentalists and theorists due to its small size, interesting excitation energy transfer (EET) properties due in part to the unique peridinin carotenoid,

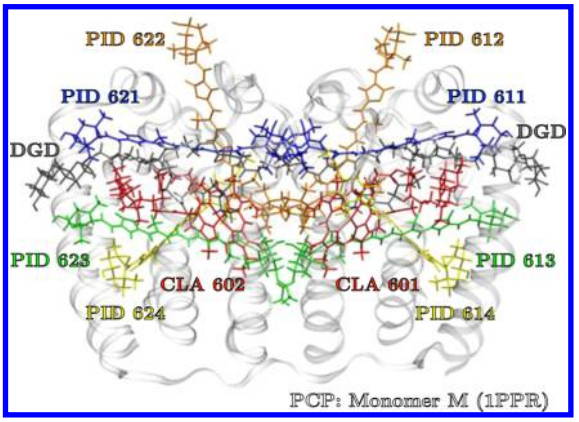

Figure 1. PCP contains two pigments—peridinin (PID) and chlorophyll *a* (CLA)—and a lipid molecule—digalactosyl diacyl glycerol (DGD). Peridinin molecules are colored based on their respective geometries, where PID611 and PID621 are blue, PID612 and PID622 are orange, PID613 and PID623 are green, and PID614 and PID624 are yellow. Chlorophyll *a* molecules are red, DGDs are gray, and the protein backbone is white. This graphic contains all molecules contained in one monomer of the PCP trimer (chain M), and all atomic coordinates are obtained from the Protein Data Bank (PDB ID 1PPR).[4] This graphic was generated using VMD.[5]

Received: February 17, 2014
Revised: July 8, 2014
Published: July 9, 2014

dx.doi.org/10.1021/jp5017054 | *J. Phys. Chem. B* 2014, 118, 9141−9154

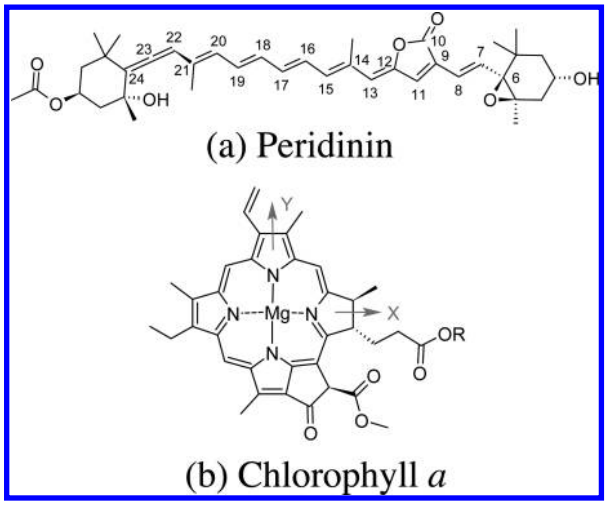

Figure 2. Two pigment molecules in PCP: peridinin and chlorophyll *a*. Carbon atoms in the peridinin polyene chain are numbered from right to left, and the phytyl tail (R) of chlorophyll *a* is not included. Standard porphyrin *x* and *y* axes are labeled.

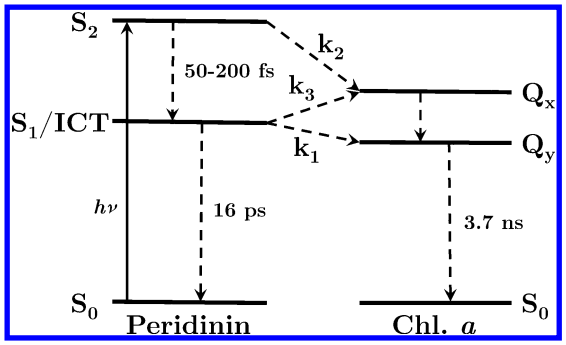

Figure 3. Excitation energy transfer pathways in PCP, with three PID to CLA pathways labeled: k_1 ($S_1 \rightarrow Q_y$), k_2 ($S_2 \rightarrow Q_x$), and k_3 ($S_1 \rightarrow Q_x$). Experimental internal conversion rates are included from $S_2 \rightarrow S_1$, $S_1 \rightarrow S_0$, and $Q_y \rightarrow S_0$. Peridinin is initially excited via the strongly allowed $S_0 \rightarrow S_2$ transition.

and high quantum efficiency (85−95%) for EET between peridinin and chlorophyll *a*.[7−9] Indeed, a recent study on PCP in the related dinoflagellate *Symbiodinium* also reported a very high peridinin to chlorophyll *a* energy transfer efficiency of 95%.[10] Furthermore, the rate of energy transfer from peridinin to chlorophyll *a* in *A. carterae* PCP has been estimated to have a lifetime of 2.3−3.2 ps.[9,11−13] The peridinin molecules surrounding the chlorophyll *a* molecules are excited from the S_0 ($1A_g^-$) ground state to the strongly allowed S_2 ($1B_u^+$) excited state, and the $S_0 \rightarrow S_1$ ($2A_g^-$) excitation is symmetry-forbidden, as is typical in similar polyenes. Once the S_2 state of peridinin is excited, EET to chlorophyll *a* via the $S_2 \rightarrow Q_x$ pathway must compete with extremely rapid internal conversion to the S_1 state in peridinin. EET via the $S_2 \rightarrow Q_x$ pathway has been previously estimated to have a transfer efficiency of only ∼25% in PCP due to an early (<200) chlorophyll *a* bleaching signature that is attributed to excitation via the peridinin S_2 excited state.[12,13] On the other hand, the rate of $S_2 \rightarrow S_1$ internal conversion in PCP has been estimated to have a lifetime of anywhere from 50 to 200 fs.[7,9,11,13] This internal conversion from $S_2 \rightarrow S_1$ has also been observed in solution, with lifetimes ranging from 30−192, depending on the polarity of the solution.[9,14] EET from the S_1 state in peridinin to chlorophyll *a* proceeds mainly via the $S_1 \rightarrow Q_y$ pathway, which competes with much slower fluorescence to the S_0 ground state in peridinin. The fluorescence lifetime of S_1 in peridinin has been estimated at around 16 ps in PCP[12,13] and is extremely solvent-dependent (ranging from 9 to 186 ps depending on the solvent polarity).[8,14,15] Additional details on the EET pathways in PCP are depicted in Figure 3.

Since solvent polarity affects the lifetime of the S_1 excited state so drastically, an intramolecular charge transfer (ICT) state in peridinin has been proposed[8,14] and confirmed as a factor in the excited state dynamics from peridinin to chlorophyll *a* in PCP.[13,16] What is unclear from these experiments is whether the ICT state acts independently of the S_1 and S_2 excited states or whether it is strongly coupled to them, thus enhancing their energy transfer properties.[17−19] It has been suggested that the ICT state is influenced by the lactone ring in peridinin, making the S_1 state in peridinin highly dependent on the solvent properties.[15,20] A recent study has shown that the ICT state develops due to S_1 and S_2 mixing, which possibly facilitates energy transfer from peridinin to chlorophyll *a*.[21]

Several computational studies have incorporated various levels of EET theory into an analysis of the PCP complex, which has been facilitated by the availability of a crystal structure of PCP in *A. carterae*, as determined by X-ray crystallography to a resolution of 2.0 A.[3] Förster resonance energy transfer (FRET) with the ideal dipole approximation (IDA) or a multipole expansion has been used to calculate the electronic interaction between transition dipole moments of donor and acceptor molecules.[22] Damjanović et al. calculated significant $S_1 \rightarrow Q_y$ transfer but none using the $S_2 \rightarrow Q_x$ pathway and a possibility of excitonically coupled S_2 states; however, they struggled to calculate accurate Coulombic couplings.[7] By reconstituting PCP with non-native chlorophyll species, Polívka et al. found that the S_1/ICT state had a lifetime of 2.7 ps in the native complex, compared to 5.9 ps (chlorophyll *b*), 2.9 ps (chlorophyll *a*), 2.2 ps (acetyl chlorophyll *a*), 1.9 ps (chlorophyll *d*), and 0.45 ps (bacteriochlorophyll *a*) in the reconstituted PCP complexes, of which all of the lifetimes were reproduced accurately using the FRET model when normalized to the energy transfer rates in the native PCP complex.[23] In pure polyene molecules, the S_1 excited state has a vanishingly small transition dipole moment due to forbidden symmetry with the ground state, and even though the peridinin molecule breaks up the polyene chain with the lactone ring and the allene group, a small but non-negligible transition dipole moment is still expected.[7] The magnitude of the S_1 transition dipole moment of peridinin has been estimated to be 0.86−3.0 D, which is small compared to the transition dipole moment of the S_2 state of peridinin, which is estimated to be 10.6−12.4 D.[7,24]

The study of EET in a light-harvesting complex necessitates appropriate theory that properly treats transitions between donor and acceptor molecules. In FRET, the transition dipole moments of a donor and acceptor molecule are coupled via a Coulombic interaction. This model is based on a weak electronic coupling between donor and acceptor molecules and carries several assumptions. First, the bath must equilibrate after donor excitation that is much faster than the rate of EET. Second, the bath coupling is greater than the donor-to-acceptor coupling. These conditions make the EET incoherent and irreversible.[25] Due to recent evidence of quantum coherence in the Fenna−Mathews−Olsen (FMO) light-harvesting com-

dx.doi.org/10.1021/jp5017054 | J. Phys. Chem. B 2014, 118, 9141−9154

plex,[26] we admit that a purely incoherent approach to EET may not take into account all of the environmental degrees of freedom. This being said, it is not clear how or to what extent quantum coherence influences the overall efficiency of energy transfer in excitation funneling processes.[27,28] The FRET model is appropriate when the transition dipole moments of a donor and acceptor molecule are coupled via a Coulombic interaction in the weak electronic coupling regime. While FRET may not explicitly include the effect of the surrounding bath (i.e., electrostatic protein environment) that contributes to the overall quantum efficiency and rectifying behavior of light-harvesting complexes,[26−28] it still provides valuable information as a baseline for calculations of energy transfer rates and efficiencies.

THEORY

The FRET model for EET was formulated from a Fermi golden rule rate expression,[29] where V_{DA} is the electronic coupling and J_{DA} is the spectral overlap between donor and acceptor excited states (eq 1):

$$k_{DA} = \frac{2\pi}{\hbar} |V_{DA}|^2 J_{DA} \tag{1}$$

The electronic coupling consists of a long-range Coulombic interaction, V_{coul}, and a short-range exchange interaction, V_{exch} (eq 2):

$$V_{DA} = V_{coul} + V_{exch} \tag{2}$$

The exchange interaction, V_{exch}, requires significant atomic orbital (AO) overlap between the donor and acceptor molecule transition densities, so it decays exponentially with distance.[30] We therefore assume that V_{exch} is negligible for this work and set $V_{DA} \approx V_{coul}$.

The FRET model[31−34] also assumes that energy transfer occurs by incoherent point dipole−point dipole interactions between pigments. This interaction is generally termed the ideal dipole approximation (IDA). V_{coul} may thus be described as follows in eq 3, using κ as an orientation factor (eq 4):

$$V_{coul} \approx V_{dip-dip} = \frac{\kappa}{4\pi\varepsilon_0} \frac{|\mu_D||\mu_A|}{R^3} \tag{3}$$

$$\kappa = \vec{\mu}_D \cdot \vec{\mu}_A - 3(\vec{\mu}_D \cdot \vec{r}_{DA})(\vec{\mu}_A \cdot \vec{r}_{DA}) \tag{4}$$

In eq 3, $V_{dip-dip}$ is the electronic−vibrational interaction energy between D and A, which is inversely proportional to the distance between the pigments and otherwise dependent on the orientation of their transition dipole moments. Two structural parameters also contribute to the energy transfer rate: R_{DA} (distance between D and A) and κ (orientation factor defined in terms of the unit vectors, $\vec{\mu}_D$ and $\vec{\mu}_A$, giving the direction of the transition dipole moments and the unit vector, $\vec{r}_{DA}$, separating their centers).

One of the main drawbacks of the FRET model is the assumption that the transitions between molecules can be treated as point dipoles; the IDA is generally valid only when the separation between donor and acceptor molecules is significantly greater than the size of the two molecules. Thus, the assumption breaks down in natural photosynthetic antennas where pigments are tightly packed within protein scaffolds. One method of increasing accuracy of the Coulombic coupling is to use a multipole expansion of the transition dipole moment along atomic centers.[25,30] Another is to generate transition densities of the donor and acceptor excited states to account for the exact electronic transition from donor to acceptor. To accomplish this, a three-dimensional grid of volume elements is created to approximate the transition densities, termed a transition density cube (TDC) and shown in eq 5. The TDCs of the donor and acceptor excited states are then summed over all coordinates to better approximate the Coulombic coupling, V_{coul}, shown in eq 6:[35,36]

$$M_{D,A}(x, y, z) = V_\delta \int_z^{z+\delta_z} \int_y^{y+\delta_y} \int_x^{x+\delta_x} \Psi_{GS}\Psi_{ES}^* \, dx \, dy \, dz \tag{5}$$

$$V_{coul} \approx V_{TDC} = \sum_{i,j} \frac{M_D(i) \, M_A(j)}{4\pi\varepsilon_0 r_{ij}} \tag{6}$$

In eq 5, the density of the ground (Ψ_{GS}) to excited (Ψ_{ES}) state transitions are calculated at a predetermined number of volume elements (where δ is the grid size and V_δ is the volume element) to form a TDC for the donor and acceptor transition density. Using eq 6, a summation is carried out over the full volumetric grid space. The only approximations involved in this calculation are the predetermined grid size and the accuracy of the quantum mechanical wave functions from which the TDCs are constructed. The TDC method, unlike the IDA method, is valid at all molecular separations and thus is well suited for EET in photosynthetic antenna systems, where pigments are tightly packed.

The second term in eq 1, J_{DA}, is the spectral overlap between donor and acceptor line shapes and is equivalent to the expression in eq 7, where A and B are normalization constants, f_D is the emission spectra, and ϵ_A is the absorption molar extinction coefficient:

$$J_{DA} = AB \int \frac{f_D(\nu)}{\nu^3} \frac{\epsilon_A(\nu)}{\nu} \, d\nu \tag{7}$$

Due to its incoherent nature, the effect of the surrounding bath is not explicitly included, which may be a limiting assumption since it is likely that the electrostatic protein environment contributes to the high quantum efficiency of antenna complexes. Nevertheless, FRET with the TDC approximation provides a baseline for calculations of energy transfer rates and efficiencies in photosynthetic antenna complexes.

COMPUTATIONAL METHODS

The availability of a high-resolution crystal structure for the PCP complex from *A. carterae* allows us to utilize a computational approach in this work. First, we use quantum mechanics to calculate the excited state absorption and emission properties of peridinin and chlorophyll *a* in PCP. Second, we utilize these excited state properties in an EET model to determine rates and efficiencies of energy transfer in PCP.

Structural Optimization of Peridinin and Chlorophyll *a* Pigments. We used the atomic coordinates of PCP in *A. carterae* that were available in the Protein Data Bank (PDB ID 1PPR)[4] and chose monomer M for our study.[3] Since crystal structures determined using X-ray diffraction do not contain hydrogen atoms, we added hydrogen atoms to the crystal structures of the peridinin (PID) and chlorophyll *a* (CLA) pigments and the digalactosyl diacyl glycerol (DGD) lipids. The protein structure was also appropriately protonated. For

dx.doi.org/10.1021/jp5017054 | J. Phys. Chem. B 2014, 118, 9141−9154

the four histidine (HIS) residues (66, 67, 229, and 230), they can be either protonated or unprotonated under physiological conditions. As shown in Figure 4, the central Mg atom in

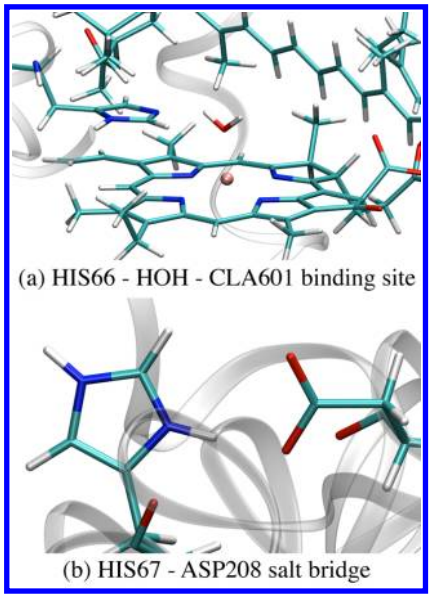

Figure 4. Two different HIS binding sites in PCP. HIS66 is unprotonated and forms a hydrogen bond with a water molecule bound to the CLA601 Mg atom. HIS67 is protonated and forms a salt bridge with ASP208. HIS229 and HIS230 are identical to HIS66 and HIS67, respectively, where HIS229 binds to a water molecule bound to the CLA602 Mg atom and HIS230 forms a salt bridge with ASP45. These images were generated using VMD.[5]

CLA601 and CLA602 is bound to a water molecule. This water molecule also forms a hydrogen bond with the HIS66 and HIS209 residues for CLA601 and CLA602, respectively.[37] For this reason, we predict that the HIS66 and HIS209 residues will remain unprotonated in PCP. On the other hand, residues HIS67 and HIS230 form a salt bridge with residues ASP208 and ASP45, respectively. For this reason, we protonate residues HIS67 and HIS230. This interaction is also shown in Figure 4. Hydrogen atoms were added to the structure of pigments, lipids, and protein using the Maestro 9.0 software.[38]

Since the hydrogen atoms were not present in the original X-ray crystal structure, these need to be optimized before any single-point quantum mechanical calculations can be performed. We optimized the geometry of all of the hydrogen atoms using the MOZYME routine[39,40] (which uses a localized molecular orbital (LMO) approximation to the typical self-consistent field (SCF) calculation) found in the MOPAC 2012 software package,[41] coupled with the semiempirical MNDO[42,43] method. These approximations were necessary due to the large number of atoms (6352) in the PCP monomer M complex. After optimization, a Mulliken population analysis[44] of the entire complex was performed so that reasonable partial charges of the environment surrounding the PCP pigments could be retained during the upcoming single-molecule excited state calculations. These initial calculations provided us with ground state geometries for the eight peridinin and two chlorophyll *a* pigments as well as an accurate electrostatic environment surrounding each pigment.

Calculation of Excited-State Properties. Even though previous researchers used time-dependent density functional theory (TD-DFT)[45,46] to calculate the excited state properties of peridinin and chlorophyll *a* in PCP and even reported evidence of the S_1 and ICT excited states,[47] it is well known that TD-DFT, which is a single-reference method,[48,49] cannot capture the S_1 excited state, which has significant double excitation character, in peridinin and related carotenoids. For this reason, we used the complete active space configuration interaction (CAS-CI),[50,51] which is a variational wave function-based method that accounts for electron correlation, to compute an approximate solution to the electronic Schrödinger equation. CAS-CI includes all configuration state functions (CSFs), such as single, double, triple, and higher excitation determinants. A recent multireference DFT study on peridinin in solvent revealed only two distinct excited states (S_1 and S_2) in the visible region, with no separate ICT state, although significant mixing of excited state character was present in differing backbone geometries.[52]

Prior to calculating excited state properties based on the ground and excited state structures, we performed two further optimization steps to prepare the ground state and excited state geometries for the calculation of vertical excitation energies using CAS-CI. It has been shown that geometries obtained from X-ray crystal structures may not be completely physically realistic for immediate use in quantum mechanical modeling, particularly the smallest bond lengths, while the distortion of the dihedral angles in the crystal structure should be fairly accurate.[53] First, the ground state CAS-CI wave functions (S_0) were optimized by freezing the dihedral angles of all of the heavy atoms in peridinin and chlorophyll *a* as well as freezing the angles and bond lengths of the heavy atoms along the peridinin polyene chain. Second, a semiconstrained optimization was performed on the excited state CAS-CI wave functions (S_1, S_2) for each peridinin molecule by freezing the dihedral angles of all of the heavy atoms in peridinin, freezing the angles and bond lengths of the carbon atoms in the two cyclohexane structures on each side of the polyene chain, and fixing two central carbon atoms (C14, C15) on the polyene chain to prevent each molecule from artificially drifting in space during the optimization. Thus, we retain the overall shape of the peridinin and chlorophyll *a* molecules from the X-ray crystal structure, while preparing them for excited state CAS-CI calculations.

The CAS-CI calculations were performed with a background electrostatic interaction[54] using the partial charges obtained from the previous Mulliken analysis of the entire PCP monomer M complex. For the optimization and excited state calculations, we used an active space of six molecular orbitals (three above and three below the HOMO−LUMO gap), performed with the MNDO semiempirical method. The results of these excited state calculations performed with CAS-CI and the MNDO method are compared in Table 2. We did not optimize the chlorophyll *a* excited states since the focus of this work is on peridinin to chlorophyll *a* and peridinin to peridinin energy transfer pathways. We thus had enough information to perform an electronic coupling analysis in PCP using the dipole−dipole approximation (eq 3), but an additional step was required to obtain the transition densities of the calculated species.

Calculation of Transition Densities. The MOPAC 2012 software used for the quantum mechanical calculation produces transition dipole moments, so EET using the dipole−dipole approximation can be modeled using the publicly available version of the software. EET calculations using the transition density cube (TDC) method, however, require the actual

dx.doi.org/10.1021/jp5017054 | J. Phys. Chem. B 2014, 118, 9141−9154

transition density of the excited state, which is not available by default. Thus, we wrote an external routine, using the Python programming language, which permutes through the configuration interaction (CI) microstates (eq 8), formed from the linear combination of Slater-type atomic orbitals (LCAO)[55] (eq 10), to construct molecular orbitals (eq 9). In this routine, we can calculate a transition density matrix in an MO basis, which is then converted to an AO basis.

$$\Psi_j = \frac{1}{\sqrt{N!}} \sum_{P=1}^{N!} (-1)^P P\left(\prod_{k=1}^{N} \psi_k^j\right) \tag{8}$$

$$\psi_i(r) = \sum_{\mu=1}^{K} C_{\mu i}\phi_\mu(r) \tag{9}$$

$$\phi_\mu(x, y, z) = \frac{(2\xi)^{n+1/2}}{\sqrt{(2n)!}} r^{n-1} \exp^{-\xi r} Y_l^m(x, y, z) \tag{10}$$

In these equations, P is the permutation operator, $C_{\mu i}$ are the AO coefficients, n is the principal quantum number (PQN), ξ is the orbital exponent, and Y_l^m are the normalized real spherical harmonics.[41,56] The transition density at each predetermined grid point can then be calculated using $P_{\mu\nu}$, the transition density matrix in the AO basis, and the AO basis set as shown in eq 11. The transition dipole moment is approximated from this transition density cube using r_i, the transition dipole moment operator, as shown in eq 12.

$$M_{nm}(x, y, z) = V_\delta \sum_{\mu\nu} P_{\mu\nu}\phi_\mu(x, y, z)\, \phi_\nu^*(x, y, z) \tag{11}$$

$$\mu_{nm} \approx \sum_i r_i M_{nm}(i) \tag{12}$$

To check the accuracy of the external transition density code, we used eq 12 to back-calculate the transition dipole moment from the TDC files of the excited state transitions. This data is shown in Table 1, where we compared the transition dipole moments back-calculated from TDCs of 0.2 Å grid size to the transition dipole moments output by MOPAC 2012. We see an average relative error of 0.0505% for the calculated grid size.

Modeling of Excitation Energy Transfer. Many of the previously published studies on energy transfer in the PCP antenna have relied on spectroscopic measurements of the overlap integral and estimations of the Coulombic coupling based on experimental transition dipoles. We instead calculated the spectra from CAS-CI vertical excitation energies both to validate experimental results and to provide a baseline of accuracy for future calculations on new systems. To calculate the spectral overlap integral, J_{DA}, we fitted ν_0 to Gaussian-type functions, shown in eq 13, where ν_0 are the vertical excitation energies and Γ_0 are the full width at half-maximum (fwhm) values for the Gaussian line shape function, and where A and B are the normalization constants for the Gaussian line shapes in eq 7.

$$\epsilon_A(\nu),\ f_D(\nu) \approx \exp\left(-2.773\left(\frac{\nu - \nu_0}{\Gamma_0}\right)^2\right) \tag{13}$$

Absolute values for ν_0 will be shown in Table 2, and these are close to experimental values but not good enough to calculate an accurate spectral overlap integral. We retained the energy differences between distinct peridinin S_1 and S_2 excited states, as these are influenced by the differing pigment geometries and protein electrostatic environments, but populated these energies instead around the following average excited state values taken from experiment, while for chlorophyll *a* Q_y and Q_x excited states we set ν_0 and Γ_0 to the following experimental values.

We used these parameters for the spectral overlap integrals: $\nu_0(S_{1,Abs})$ = 16 694, $\nu_0(S_{1,Em})$ = 13 986, $\nu_0(S_{2,Abs})$ = 20 661, $\nu_0(S_{2,Em})$ = 19 170, $\nu_0(Q_{y,Abs})$ = 14 993, $\nu_0(Q_{x,Abs})$ = 16 000, $\Gamma_0(S_{1,Abs})$ = 4247, $\Gamma_0(S_{1,Em})$ = 2967, $\Gamma_0(S_{2,Abs})$ = 4315, $\Gamma_0(S_{2,Em})$ = 3709, $\Gamma_0(Q_{y,Abs})$ = 270, and $\Gamma_0(Q_{x,Abs})$ = 1025 . Peridinin $S_{1,Em}$ parameters were based on spectra in *n*-hexane

Table 1. Comparison of Dipole Moments Calculated from Transition Density Cubes (TDCs) Using a 0.2 Å Grid Size[a]

		absorption		exact
		μ_{12}	error	μ_{12}
molecule	ES	(D)	(%)	(D)
PID611	S_1	1.4474	0.0483	1.4481
	S_2	17.6553	0.0623	17.6443
PID612	S_1	4.2498	0.0259	4.2509
	S_2	17.2530	0.0000	17.2530
PID613	S_1	4.8245	0.0207	4.8255
	S_2	16.9380	0.0100	16.9397
PID614	S_1	1.0697	0.3095	1.0664
	S_2	18.4058	0.0005	18.4057
PID621	S_1	0.6866	0.1600	0.6877
	S_2	16.7769	0.0370	16.7707
PID622	S_1	6.1391	0.0196	6.1379
	S_2	16.0845	0.0765	16.0722
PID623	S_1	3.2805	0.0427	3.2791
	S_2	17.1884	0.0070	17.1896
PID624	S_1	12.9896	0.0192	12.9871
	S_2	8.7419	0.0515	8.7374
CLA601	Q_y	3.5592	0.0225	3.5584
	Q_x	0.4535	0.0883	0.4531
CLA602	Q_y	3.6519	0.0411	3.6534
	Q_x	0.3559	0.0842	0.3562
		emission		exact
		μ_{12}	error	μ_{12}
molecule	ES	(D)	(%)	(D)
PID611	S_1	0.2540	0.0787	0.2542
	S_2	16.6048	0.0928	16.5894
PID612	S_1	3.9722	0.0025	3.9723
	S_2	15.8200	0.0145	15.8177
PID613	S_1	1.0237	0.0781	1.0245
	S_2	16.8159	0.0339	16.8102
PID614	S_1	0.2719	0.0736	0.2717
	S_2	16.7589	0.0423	16.7660
PID621	S_1	1.2366	0.0647	1.2358
	S_2	16.5039	0.0121	16.5059
PID622	S_1	4.2542	0.0659	4.2514
	S_2	15.4412	0.0175	15.4439
PID623	S_1	1.0468	0.0000	1.0468
	S_2	16.4418	0.0517	16.4503
PID624	S_1	2.6350	0.0456	2.6338
	S_2	15.7382	0.0172	15.7409

[a]All calculations use CAS-CI with the MNDO method and an active space of six MOs. Percent errors in TDC dipole moments are calculated relative to the exact calculated dipole moment in the last column.

dx.doi.org/10.1021/jp5017054 | J. Phys. Chem. B 2014, 118, 9141−9154

Table 2. Excited State Absorption and Emission Properties for Peridinin and Chlorophyll *a* Species in PCP Using CAS-CI with an Active Space of Six Molecular Orbitals and the MNDO Semiempirical Method[a]

		absorption properties			
		E	μ_{12}	S	D
molecule	ES	(eV)	(D)	(%)	(%)
PID611	S_1	2.12	1.45	22.64	60.28
	S_2	2.38	17.64	89.85	7.12
PID612	S_1	2.10	4.25	26.55	57.19
	S_2	2.43	17.25	85.11	10.89
PID613	S_1	2.14	4.83	28.16	56.55
	S_2	2.41	16.94	84.94	11.24
PID614	S_1	2.01	1.07	21.54	59.86
	S_2	2.34	18.41	89.50	7.35
PID621	S_1	2.35	0.69	23.12	62.08
	S_2	2.50	16.77	91.76	5.50
PID622	S_1	2.24	6.14	32.72	53.39
	S_2	2.51	16.07	81.81	13.64
PID623	S_1	2.15	3.28	24.86	58.45
	S_2	2.41	17.19	89.28	7.98
PID624	S_1	2.44	12.99	70.75	23.24
	S_2	2.55	8.74	49.10	42.84
CLA601	Q_y	2.07	3.56	90.20	7.04
	Q_x	2.18	0.45	79.97	14.54
CLA602	Q_y	2.02	3.65	93.54	4.48
	Q_x	2.16	0.36	77.81	14.81
		emission properties			
		E	μ_{12}	S	D
molecule	ES	(eV)	(D)	(%)	(%)
PID611	S_1	1.56	0.25	16.80	57.41
	S_2	2.45	16.59	86.05	10.70
PID612	S_1	1.60	3.97	19.98	54.95
	S_2	2.53	15.82	80.13	15.35
PID613	S_1	1.49	1.02	16.47	56.56
	S_2	2.34	16.81	81.73	14.69
PID614	S_1	1.57	0.27	17.09	56.87
	S_2	2.42	16.77	84.45	12.09
PID621	S_1	1.57	1.24	16.85	57.99
	S_2	2.49	16.51	89.66	7.64
PID622	S_1	1.60	4.25	19.83	55.57
	S_2	2.53	15.44	77.76	17.54
PID623	S_1	1.55	1.05	16.97	56.99
	S_2	2.49	16.45	91.88	5.99
PID624	S_1	1.50	2.63	18.21	55.65
	S_2	2.44	15.74	88.42	8.94

[a]Single (S) and double (D) excitation percentages are shown.

and used to estimate peridinin $S_{1,Abs}$ parameters, peridinin S_2 and chlorophyll *a* parameters were estimated from spectra in PCP, and fwhm values were estimated from experimental spectra and previous FRET studies.[3,7−9,11−15] To simplify the model, vibrational bands were not included, although the vertical energy for $S_{1,Em}$ corresponds to the (0−2) vibronic band, which is generally the maximum for S_1 fluorescence in carotenoids.[14,57] The energies and oscillator strengths of the CAS-CI calculations for the S_2 absorption and emission excited states in this study correspond to the (0−0) vibronic band, so electronic couplings involving these S_1 states may in fact be weaker than in the actual system. We acknowledge that the choice of spectral overlap parameters for PCP is difficult, especially for the S_1 absorption and emission and the Q_x absorption, since there is no consensus on where these peaks should lie. Several two-photon absorption studies have even speculated that the S_1 state may lie closer to the S_2 state in PCP than is found in solution.[17,58,59] The parameters chosen are thus partially based on analysis of PCP spectra and partially based on the analysis of pigment spectra in solvent. Spectral overlap calculations will be compared in Tables 4 and 6.

To calculate the electronic coupling term, V_{DA}, we constructed a transition density cube file (in Gaussian cube file format) for the fluorescence transition density of the donor molecules and the absorption transition density for the acceptor molecules from their respective transition density matrix elements using the Python code previously mentioned. The electronic coupling between these excited state transitions was estimated using the transition density cube (TDC) method.[35,36] Electronic coupling calculations, comparing the IDA and TDC (using a grid size of 0.2 Å^3), will be compared in Tables 3 and 5.

RESULTS AND DISCUSSION

Since our EET analysis is based entirely on excited state properties of peridinin and chlorophyll *a* which are calculated from the complete active space configuration interaction (CAS-CI), we must ensure that our calculated excited states very closely approximate those found in the natural PCP antenna. We thus compare excited state energies, transition dipole moments, and excited state symmetries to available experimental values, which provide a reference for evaluating the accuracy of the calculated properties.

Pigment Geometry. In Figure 5, we compare the ground state geometries of the eight peridinin species in PCP. The ground state configuration of the polyene chain in peridinin, which includes an allene group on the left side and a lactone ring on the right side, varies between all pigments considered; all of the polyene chains are bent, which is due to the local environment and protein electrostatics. The shape of the polyene chain differs among the eight peridinin molecules shown, although the geometry is similar among pairs PID611 and PID621, PID612 and PID622, PID613 and PID623, and PID614 and PID624. The shape of the peridinin molecules was retained during S_1 and S_2 excited state optimizations since the dihedral angles of the heavy atoms were kept frozen. CLA601 and CLA602 are nearly identical in geometry, and we do not optimize the chlorophyll *a* excited states in this study so these are not shown.

Figure 6 compares the ground state and excited state C−C bond lengths in peridinin species along the polyene chain as labeled in Figure 2. In Figure 6a, the bond lengths in the peridinin X-ray crystal structures are compared to a peridinin molecule fully optimized at the B3LYP/6−31+g(d) level of theory[60−63] using Gaussian 09.[64] We note the large effect that the protein electrostatic environment has on the structure of each peridinin molecule, as the bond lengths vary widely between species. In contrast, since the C−C bond lengths in peridinin were allowed to optimize prior to the S_1 and S_2 excited state calculations, Figure 6b,c show a fairly homogeneous picture when comparing peridinin species.

In the FRET model, the distance between donor and acceptor molecules is very important since the rate scales by a factor of $1/R_{DA}^6$, as derived from Coulomb's law of electrostatics. In EET between peridinin and chlorophyll *a* molecules, the closest R_{DA} values—between PID614 and CLA601 and

dx.doi.org/10.1021/jp5017054 | J. Phys. Chem. B 2014, 118, 9141−9154

Table 3. Comparison of Dipole−Dipole and TDC Coulombic Couplings (V_{DA}) between Peridinin and Chlorophyll *a* Using CAS-CI with the MNDO Semiempirical Method and an Active Space of Six MOs[a]

			R_{DA}		V_{DA} (eV)		J_{DA}
	donor	acceptor	(Å)	κ	dipole−dipole	TDC: 0.2 Å^3	(eV^{-1})
$S_1 \rightarrow Q_y$	PID611	CLA601	10.77	−0.066	-2.96×10^{-5}	-4.00×10^{-4}	1.509
	PID612	CLA601	11.99	0.476	2.44×10^{-3}	4.61×10^{-3}	1.852
	PID613	CLA601	11.64	−1.741	-2.51×10^{-3}	-4.41×10^{-3}	0.822
	PID614	CLA601	6.57	−1.002	-2.13×10^{-3}	3.49×10^{-3}	1.556
	PID621	CLA602	10.21	−1.103	-2.93×10^{-3}	-2.36×10^{-3}	1.573
	PID622	CLA602	12.33	−0.819	-4.24×10^{-3}	-4.42×10^{-3}	1.847
	PID623	CLA602	11.45	−1.278	-2.03×10^{-3}	-8.47×10^{-5}	1.362
	PID624	CLA602	8.54	0.609	5.88×10^{-3}	-1.28×10^{-4}	0.921
$S_1 \rightarrow Q_x$	PID611	CLA601	10.23	−0.583	-3.91×10^{-5}	-2.18×10^{-5}	0.564
	PID612	CLA601	11.52	−0.995	-7.33×10^{-4}	1.06×10^{-4}	0.796
	PID613	CLA601	11.56	−0.087	-1.63×10^{-5}	-6.36×10^{-4}	0.232
	PID614	CLA601	6.44	−0.216	-6.21×10^{-5}	-3.69×10^{-5}	0.592
	PID621	CLA602	9.62	−0.913	-2.81×10^{-4}	-8.19×10^{-5}	0.603
	PID622	CLA602	11.65	−0.691	-8.34×10^{-4}	-8.21×10^{-4}	0.792
	PID623	CLA602	11.14	−0.712	-1.20×10^{-4}	3.15×10^{-5}	0.480
	PID624	CLA602	8.24	−0.869	-9.08×10^{-4}	4.51×10^{-5}	0.271
$S_2 \rightarrow Q_x$	PID611	CLA601	10.21	−1.202	-5.31×10^{-3}	2.45×10^{-3}	0.529
	PID612	CLA601	10.82	0.779	2.75×10^{-3}	1.09×10^{-3}	0.248
	PID613	CLA601	10.66	0.514	2.02×10^{-3}	-4.32×10^{-3}	1.091
	PID614	CLA601	6.86	−1.094	-1.61×10^{-2}	-1.28×10^{-3}	0.654
	PID621	CLA602	9.97	−1.103	-4.08×10^{-3}	1.65×10^{-3}	0.388
	PID622	CLA602	10.73	0.648	1.80×10^{-3}	-3.18×10^{-4}	0.256
	PID623	CLA602	11.02	−0.752	-2.05×10^{-3}	4.05×10^{-3}	0.375
	PID624	CLA602	7.06	1.021	1.01×10^{-2}	-2.81×10^{-4}	0.564

[a]Spectral overlap integrals (J_{DA}) are compared in the last column.

Table 4. Rates (k_{DA}), Lifetimes (τ_{DA}), and Efficiencies (Φ_{DA}) of EET Compared between Peridinin and Chlorophyll *a* Using Both the Dipole−Dipole and TDC Methods to Calculate the Coulombic Coupling (V_{DA}), Where $\tau_{DA} = k_{DA}^{-1}$

			dipole−dipole coupling			TDC coupling		
			k_{DA}	τ_{DA}	Φ_{DA}	k_{DA}	τ_{DA}	Φ_{DA}
	donor	acceptor	(ps^{-1})	(ps)	(%)	(ps^{-1})	(ps)	(%)
$S_1 \rightarrow Q_y$	PID611	CLA601	1.27×10^{-5}	79000	0.02	2.31×10^{-3}	433	3.56
	PID612	CLA601	1.05×10^{-1}	9.53	62.67	3.76×10^{-1}	2.66	85.75
	PID613	CLA601	4.95×10^{-2}	20.2	44.20	1.52×10^{-1}	6.56	70.91
	PID614	CLA601	6.74×10^{-2}	14.8	51.87	1.80×10^{-1}	5.54	74.27
	PID621	CLA602	1.28×10^{-1}	7.79	67.26	8.39×10^{-2}	11.9	57.30
	PID622	CLA602	3.16×10^{-1}	3.16	83.50	3.45×10^{-1}	2.90	84.65
	PID623	CLA602	5.38×10^{-1}	18.6	46.24	9.32×10^{-5}	10700	0.15
	PID624	CLA602	3.04×10^{-1}	3.29	82.95	1.45×10^{-2}	69.2	18.79
$S_1 \rightarrow Q_x$	PID611	CLA601	8.24×10^{-6}	121000	0.01	2.55×10^{-6}	392000	0.00
	PID612	CLA601	4.08×10^{-3}	245	6.13	8.61×10^{-5}	11600	0.14
	PID613	CLA601	5.85×10^{-7}	1710000	0.00	8.95×10^{-4}	1120	1.41
	PID614	CLA601	2.18×10^{-5}	45900	0.03	7.69×10^{-6}	130000	0.01
	PID621	CLA602	4.56×10^{-4}	2190	0.72	3.86×10^{-5}	25900	0.06
	PID622	CLA602	1.92×10^{-3}	520	2.99	1.81×10^{-3}	554	2.81
	PID623	CLA602	6.58×10^{-5}	15200	0.11	4.54×10^{-6}	220000	0.01
	PID624	CLA602	2.13×10^{-3}	469	3.30	5.28×10^{-6}	190000	0.01
$S_2 \rightarrow Q_x$	PID611	CLA601	1.42×10^{-1}	7.03	2.76	3.03×10^{-2}	33.0	0.60
	PID612	CLA601	1.79×10^{-2}	55.9	0.36	2.83×10^{-3}	353	0.06
	PID613	CLA601	4.24×10^{-2}	23.6	0.84	1.95×10^{-1}	5.14	3.74
	PID614	CLA601	1.61	0.621	24.36	1.03×10^{-2}	97.3	0.21
	PID621	CLA602	6.16×10^{-2}	16.2	1.22	1.01×10^{-2}	98.9	0.20
	PID622	CLA602	7.94×10^{-3}	126	0.16	2.47×10^{-4}	4050	0.00
	PID623	CLA602	1.51×10^{-2}	66.2	0.30	5.87×10^{-2}	17.1	1.16
	PID624	CLA602	5.53×10^{-1}	1.81	9.96	4.26×10^{-4}	2350	0.01

dx.doi.org/10.1021/jp5017054 | J. Phys. Chem. B 2014, 118, 9141−9154

Table 5. Comparison of Dipole−Dipole and TDC Coulombic Couplings (V_{DA}) between Peridinin and Peridinin Using CAS-CI with the MNDO Semiempirical Method and an Active Space of Six MOs[a]

			R_{DA}		V_{DA} (eV)		J_{DA}
	donor	acceptor	(A)	κ	dipole−dipole	TDC: 0.2 A^3	(eV^{-1})
$S_1 \rightarrow S_1$	PID611	PID612	6.09	−0.040	-1.20×10^{-4}	1.13×10^{-3}	0.839
	PID612	PID622	16.31	1.153	4.05×10^{-3}	3.19×10^{-3}	0.524
	PID613	PID612	14.22	1.179	1.11×10^{-3}	7.29×10^{-4}	0.602
	PID614	PID613	8.91	0.681	7.88×10^{-4}	-6.10×10^{-4}	0.741
	PID621	PID622	5.96	0.732	1.64×10^{-2}	3.41×10^{-3}	0.447
	PID622	PID612	16.37	1.149	2.96×10^{-3}	2.30×10^{-3}	0.953
	PID623	PID622	14.42	−1.018	-1.36×10^{-3}	-1.03×10^{-3}	0.394
	PID624	PID623	7.00	−0.629	-9.88×10^{-3}	-1.95×10^{-3}	0.512
$S_2 \rightarrow S_2$	PID611	PID612	6.09	−0.389	-3.09×10^{-1}	-8.43×10^{-2}	1.004
	PID612	PID611	6.04	0.487	3.85×10^{-1}	1.03×10^{-1}	1.254
	PID613	PID614	8.20	0.396	1.39×10^{-1}	5.71×10^{-2}	0.948
	PID614	PID613	8.02	−0.468	1.61×10^{-1}	-5.61×10^{-2}	0.981
	PID621	PID622	6.18	−0.489	-3.43×10^{-1}	-7.40×10^{-2}	0.874
	PID622	PID621	5.94	0.531	-4.10×10^{-1}	8.13×10^{-2}	1.023
	PID623	PID624	8.34	−0.298	-6.84×10^{-2}	-3.98×10^{-2}	1.059
	PID624	PID623	8.00	0.367	1.21×10^{-1}	4.91×10^{-2}	1.019

[a]Spectral overlap integrals (J_{DA}) are compared in the last column. The largest Coulombic coupling is shown for each PID donor.

Table 6. Rates (k_{DA}), Lifetimes (τ_{DA}), and Efficiencies (Φ_{DA}) of EET Compared between Peridinin Molecules Using Both the Dipole−Dipole and TDC Methods to Calculate the Coulombic Coupling (V_{DA}), where $\tau_{DA} = k_{DA}^{-1}$[a]

			dipole−dipole coupling			TDC coupling		
			k_{DA}	τ_{DA}	Φ_{DA}	k_{DA}	τ_{DA}	Φ_{DA}
	donor	acceptor	(ps^{-1})	(ps)	(%)	(ps^{-1})	(ps)	(%)
$S_1 \rightarrow S_1$	PID611	PID612	1.16×10^{-4}	8650	0.18	1.03×10^{-2}	97.4	14.11
	PID612	PID622	8.19×10^{-2}	12.2	56.71	5.09×10^{-2}	19.7	44.87
	PID613	PID612	7.10×10^{-3}	141	10.20	3.05×10^{-3}	328	4.65
	PID614	PID613	4.39×10^{-3}	228	6.57	2.63×10^{-3}	380	4.04
	PID621	PID622	1.15	0.871	94.84	4.96×10^{-2}	20.2	44.23
	PID622	PID612	7.96×10^{-2}	12.6	56.02	4.80×10^{-2}	20.8	43.45
	PID623	PID622	6.97×10^{-3}	144	10.03	4.02×10^{-3}	249	6.04
	PID624	PID623	4.77×10^{-1}	2.10	88.42	1.86×10^{-2}	53.8	22.93
			(fs^{-1})	(fs)	(%)	(fs^{-1})	(fs)	(%)
$S_2 \rightarrow S_2$	PID611	PID612	9.13×10^{-1}	1.10	99.46	6.81×10^{-2}	14.7	93.16
	PID612	PID611	1.77	0.565	99.72	1.26×10^{-1}	7.96	96.17
	PID613	PID614	1.74×10^{-1}	5.74	97.21	2.96×10^{-2}	33.8	85.53
	PID614	PID613	2.43×10^{-1}	4.12	97.98	2.95×10^{-2}	33.9	85.50
	PID621	PID622	9.81×10^{-1}	1.02	99.49	4.56×10^{-2}	21.9	90.13
	PID622	PID621	1.64	0.609	99.70	6.46×10^{-2}	15.5	92.82
	PID623	PID624	4.74×10^{-2}	21.1	90.45	1.60×10^{-2}	62.4	76.23
	PID624	PID623	1.43×10^{-1}	7.01	96.61	2.34×10^{-2}	42.7	82.42

[a]Only peridinin pairs with the largest Coulombic couplings are shown as calculated in Table 4.

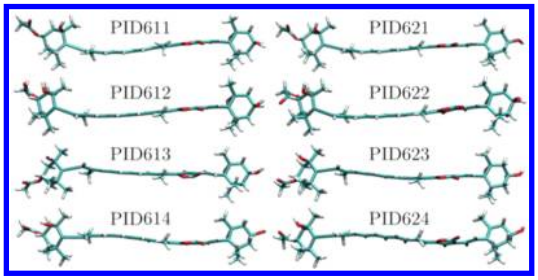

Figure 5. Relative ground state (S_0) geometries of peridinin molecules in PCP from the X-ray crystal structure (1PPR). These images were generated using VMD.[5]

between PID624 and CLA602—are around 6−8 Å. The other interactions between peridinin and chlorophyll *a* are around 10−12 Å. The values for all of these R_{DA} values are shown in Tables 3 and 5. EET between two peridinin molecules is expected to be most efficient between the following pigment pairs that are closest spatially: PID611 and PID612 (6 Å apart), PID613 and PID614 (6 Å apart), PID621 and PID622 (8 Å apart), and PID623 and PID624 (8 Å apart). The remaining pigment pairs are 10−32 Å apart. On the basis of these values, EET between peridinin and chlorophyll *a* might be expected to be most efficient between PID614 and CLA601 and between PID624 and CLA602 as long as their respective transition densities are in resonance.

dx.doi.org/10.1021/jp5017054 | J. Phys. Chem. B 2014, 118, 9141−9154

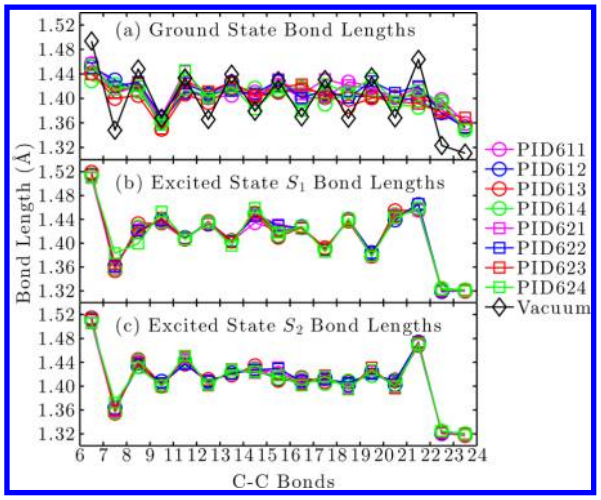

Figure 6. Bond lengths along the conjugated carbon chain in peridinin. (a) Relative bond lengths (Å) of peridinin molecules in PCP from the X-ray crystal structure (1PPR) compared to peridinin optimized in vacuum using B3LYP/6−31+g(d). (b) Relative bond lengths (Å) of the S_1 excited state of peridinin in PCP optimized using CAS-CI/MNDO. (c) Relative bond lengths (Å) of the S_2 excited state of peridinin in PCP optimized using CAS-CI/MNDO.

Excited-State Properties. In Table 2, we list the calculated absorption/emission properties for peridinin and chlorophyll *a* species in PCP, along with their respective transition dipole moments and their percentage of single/double excitation character, and Figure 7 compares the energies of the CAS-CI

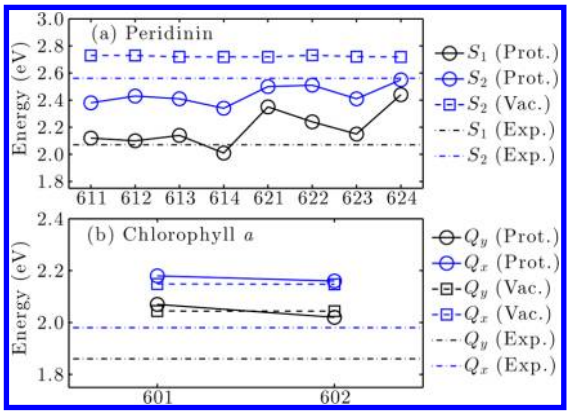

Figure 7. Calculated excited state energies of peridinin and chlorophyll *a* species in PCP and vacuum compared to experimental values. (a) Peridinin excited state absorption energies using CAS-CI compared to peridinin fully optimized in vacuum using B3LYP/6−31+g(d). (b) Chlorophyll *a* excited state absorption energies using CAS-CI compared to chlorophyll *a* fully optimized in vacuum using B3LYP/6−31+g(d). All calculations were carried out with the MNDO semiempiricial method and an active space of six molecular orbitals.

calculations for the eight peridinin and two chlorophyll *a* molecules to peridinin and chlorophyll *a* molecules first optimized in vacuum using B3LYP/6−31+g(d). The vacuum-optimized peridinin has a planar polyene chain structure and does not retain the doubly excited S_1 excited state. Thus, we demonstrate the importance of keeping the dihedral angles frozen during peridinin ground and excited state optimizations. This is in contrast to the Q_y and Q_x excited states in chlorophyll *a*, which are more robust and do not vary significantly even when fully optimized in vacuum.

Excited state energies can be compared to the experimental averages that we use for our spectral overlap calculations: $S_{1,Abs}$ = 2.07, $S_{1,Em}$ = 1.73, $S_{2,Abs}$ = 2.56, $S_{2,Em}$ = 2.38, $Q_{y,Abs}$ = 1.86, and $Q_{x,Abs}$ = 1.98. On the basis of these experimental energies, we see that most of the peridinin S_1 absorption energies are slightly higher than the experimental value, except for PID614, and all of the peridinin S_2 absorption energies are lower than the experimental average. A notable exception is the absorption profile of PID624, which has two S_2-like states, since the double-excitation character of both is less than 50%. When the S_1 state of PID624 is optimized, it emits with significantly more double-excitation character. The peridinin S_1 emission energies are significantly lower than the average, and the S_2 emission energies are close to the experimental values but are slightly higher in energy. The chlorophyll *a* Q_y and Q_x absorption energies correspond well to the experimental energy gap, but they are both slightly higher than the experimental average. Since some excited state energy values are higher and others are lower than experimental averages, an accurate calculation of the spectral overlap integral becomes difficult without linearly extrapolating the raw energy data.

Calculated transition dipole moments are compared to estimated values of 0.86−3.0 D for S_1, 10.6−12.4 D for S_2, 5.2 D for Q_y, and 3.5 D for Q_x.[7,65] These estimated values all appear reasonably close to experimental values except that the Q_x value may be overestimated since it has not been measured experimentally and furthermore is difficult to detect in PCP spectra. The calculated transition dipole moments for peridinin S_1 absorption and emission are all relatively close to the estimated values, except again for the S_1 absorption of PID624, which is more S_2-like in character. PID612, PID613, PID622, and PID623 are also above the estimated upper limit of 3.0 D for S_1 absorption, a discrepancy since S_1 absorption is not visible in any experimental spectra. However, upon S_1 excited state optimization only PID612 and PID622 remain greater than 3.0 D, contributing to their greater respective Coulombic couplings shown in Table 3. The calculated transition dipole moments for peridinin S_2 absorption and emission are all higher than the estimated values. The calculated transition dipole moments for chlorophyll *a* Q_y and Q_x are both lower than the estimated values but are reasonable when compared relative to each other. Since the magnitude of the transition dipole moment is an indicator of the Coulombic coupling strength, we may expect transitions involving the S_2 and S_1 states to be slightly overestimated and transitions involving both the Q_y and Q_x states to be slightly underestimated. These factors are offsetting when calculating PID → CLA couplings, but it is difficult to determine whether the transition dipole moment errors will cancel each other out without more accurate experimental transition dipole information.

Our calculated S_1 transitions, both absorption and emission, show roughly 50−60% double excitation character, compared to the roughly 80−90% single excitation character of the S_2 transitions. Both Q_y and Q_x transitions have significant (80−90%) single excitation character. This is significant since these transitions can be distinguished based on this characteristic alone. The transition densities of peridinin and chlorophyll *a*, shown in Figures 8 and 9, do not directly show the wave function symmetry of the S_0, S_1, S_2, Q_y, and Q_x ground and excited states, but they show the magnitude and direction of electron density movement upon absorption or emission of a photon.

dx.doi.org/10.1021/jp5017054 | J. Phys. Chem. B 2014, 118, 9141−9154

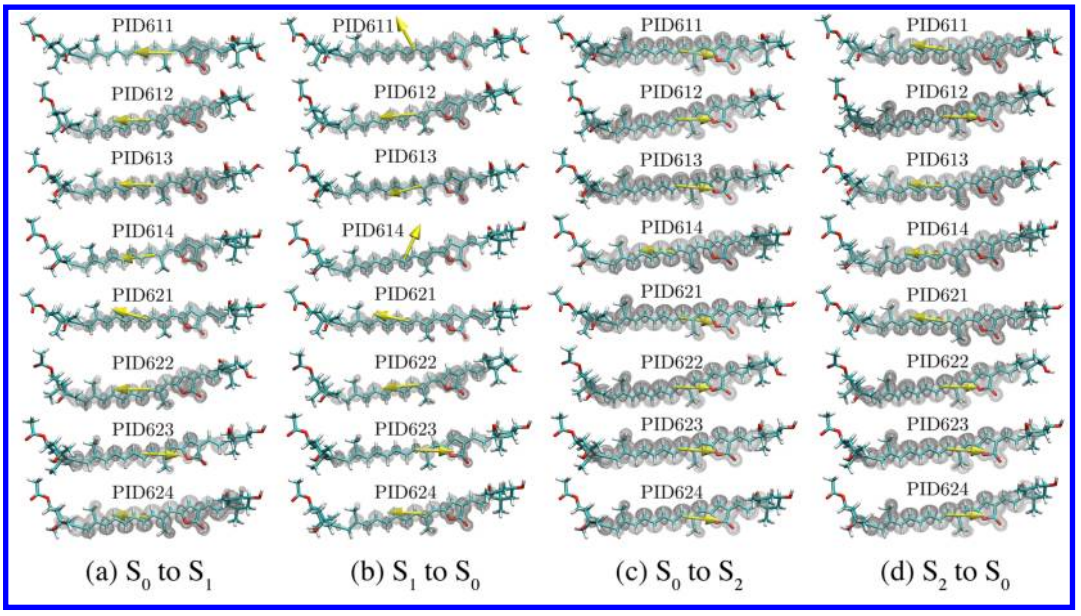

Figure 8. Transition densities of eight peridinin molecules in PCP vertically excited from the ground state and excited state geometries. (a) Transition density of the $S_0 \rightarrow S_1$ excited state absorption, where electron density is moving from light gray to dark gray. (b) Transition density of the $S_1 \rightarrow S_0$ excited state emission. (c) Transition density of the $S_0 \rightarrow S_2$ excited state absorption. (d) Transition density of the $S_2 \rightarrow S_0$ excited state emission. The yellow arrows represent the direction of normalized transition dipole moment vectors from the center of transition charge density. These images were generated using VMD, with a density isovalue of 0.00005.[5]

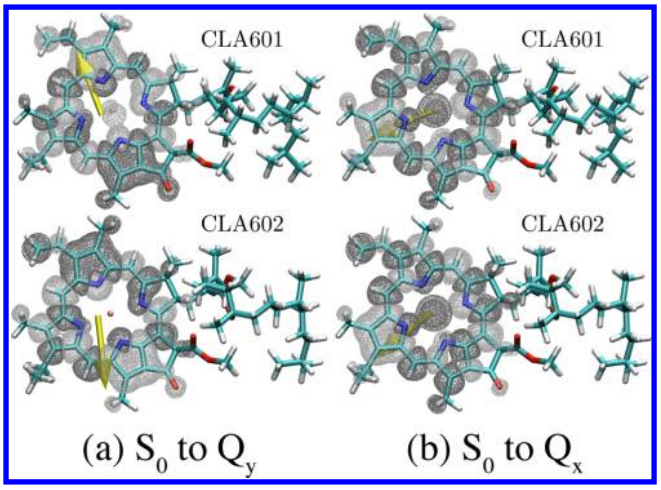

Figure 9. Transition densities of two chlorophyll *a* molecules in PCP vertically excited from the ground state geometries. (a) Q_y absorption transition density for the chlorophyll *a* 601 and 602 molecules, where the electron density moves from light gray to dark gray. (b) Q_x absorption transition density for the chlorophyll *a* 601 and 602 molecules. The yellow arrows represent the direction of normalized transition dipole moment vectors from the center of transition charge density. These images were generated using VMD, and the isovalue used to generate the transition densities was 0.00005.[5]

The absorption and emission transition density of the peridinin S_2 excited state is a strongly allowed transition with clear symmetry along the π-conjugated polyene chain. The absorption and emission transition density of the peridinin S_1 excited state, on the other hand, is not as strongly allowed and has some symmetry along the π-conjugated polyene chain, but the symmetry is broken up in some cases by the lactone ring. This broken symmetry adds an element of intramolecular charge transfer (ICT), which can be clearly noted in the emission of PID612 and PID622 but not in the emission of PID611 and PID614. The direction of the transition dipole moment (shown as a yellow arrow) should correlate with the amount of ICT character of the excited state. Thus, a peridinin excited state with strong ICT characteristics should have a transition dipole moment directed close to parallel to the polyene chain. The localization of the ICT character due to the lactone ring in the peridinin S_1 excited state has been suggested in previous studies.[15] Since peridinin is not a pure polyene, in that its symmetry is broken by the allene group and the lactone ring, we do not expect the $S_0 \rightarrow S_1$ transition to be completely optically forbidden. In fact, this transition has a mixture of characteristics, including those of the allowed $S_0 \rightarrow S_2$ transition, and some ICT behavior.

We look at the major electronic configurational contributions to each excited state to determine if the calculated electronic structure conforms to theory. Since we used an active space of six MOs (three above and three below the HOMO−LUMO gap), we represent the ground state electronic configuration as [2 2 2 0 0 0]. The major contribution to the peridinin S_2 excited state manifold is the singly excited [2 2 1 1 0 0] configuration, which accounts for 79.38, 68.02, 68.82, and 80.06% in the PID611, PID612, PID613, and PID614 S_2 absorption configurations and 72.92, 58.00, 67.60, and 70.24% in the PID611, PID612, PID613, and PID614 S_2 emission configurations, respectively. There are no other major contributions to the S_2 excited states. The S_1 excited state configurational manifold, on the other hand, is more interesting. The doubly excited [2 2 0 2 0 0] configuration is the largest contribution and accounts for 31.75, 28.53, 26.86, and 31.32% in the PID611, PID612, PID613, and PID614 S_1 absorption configurations and 30.13, 26.67, 27.80, and 29.43% in the PID611, PID612, PID613, and PID614 S_1 emission configurations, respectively. Other major contributions to the electronic configuration of the S_1 excited state are the ground state [2 2 2 0 0 0], doubly excited [2 1 1 1 1 0], [2 2 0 1 1 0], and singly excited [2 2 1 1 0 0], [2 2 1 0 1 0], [2 1 2 1 0 0]

dx.doi.org/10.1021/jp5017054 | J. Phys. Chem. B 2014, 118, 9141−9154

configurations. The S_1 excited state in peridinin, therefore, is not a pure double excitation ([2 2 0 2 0 0]), as would be expected in a completely symmetric polyene, but consists of a number of configurations, including singly excited configurations, which are also found in the S_2 excited state. These similarities between the S_1 and S_2 configurational manifold may explain the extremely fast relaxation from $S_2 \rightarrow S_1$ and the partially allowed $S_0 \rightarrow S_1$ transition.

The CLA601 transition densities for the $S_0 \rightarrow Q_y$ and $S_0 \rightarrow Q_x$ transitions are shown in Figure 9, and we note that in the $S_0 \rightarrow Q_y$ transition, electron density moves along the *y* axis of the porphyrin ring and in the $S_0 \rightarrow Q_x$ transition, electron density moves along the *x* axis of the porphyrin ring, conforming to the convention shown in Figure 2.[66] We can also look at the major configurational contributions for the Q_y and Q_x excited states and determine if they conform to the Gouterman four-orbital model, where the Q_y excited state is dominated by the [2 1 1 0] and [1 2 0 1] singly excited configurations and the Q_x excited state is dominated by the [1 2 1 0] and [2 1 0 1] singly excited configurations.[67] The major contribution to the Q_y excited state manifold is the [2 2 1 1 0 0] singly excited configuration, which accounts for 64.64% in CLA601 and 67.34% in CLA602. The only other major contribution is from the [2 1 2 0 1 0] singly excited configuration, which accounts for 23.14% in CLA601 and 23.72% in CLA602. Two relatively equal configurations dominate the Q_x excited states, which are the [2 2 1 0 1 0] singly excited configuration, which accounts for 38.79% in CLA601 and 37.76% in CLA602, and the [2 1 2 1 0 0] singly excited configuration, which accounts for 38.72% in CLA601 and 38.56% in CLA602. This data conforms very well to the Gouterman four-orbital model, accounting for roughly 80−90% of the configurations in the Q_y and Q_x excited state manifolds.

Peridinin → Chlorophyll *a* EET. In Table 3, we compare the Coulombic couplings, V_{DA}, and spectral overlap integrals, J_{DA}, for the three pathways of peridinin to chlorophyll *a* EET studied in this paper: $S_1 \rightarrow Q_y$, $S_1 \rightarrow Q_x$, and $S_2 \rightarrow Q_x$. The couplings between $S_1 \rightarrow Q_y$ and $S_2 \rightarrow Q_x$ pathways are roughly the same order of magnitude, while the coupling between $S_1 \rightarrow Q_x$ is smaller by roughly an order of magnitude. It is important to note that the Coulombic coupling calculated using the dipole−dipole approximation is not a good approximation for the full TDC interaction. In one case, the dipole−dipole approximation is almost 2 orders of magnitude larger than the TDC interaction (i.e., PID623 $S_1 \rightarrow$ CLA602 Q_y). This will lead to significant errors in the EET modeling since the V_{DA} term is squared. Spectral overlap terms are roughly consistent within the separate EET pathways, with $S_1 \rightarrow Q_y$ exhibiting the highest overlaps, as expected.

In Table 4, we compare the rates, lifetimes, and efficiencies of these pathways as calculated using the EET equation (eq 1). The $S_1 \rightarrow Q_y$ pathway is by far the most efficient of the three pathways considered, and the transfer is dominated specifically by PID612 to CLA601 and PID622 to CLA602, with lifetimes of 2.66 ps and 2.90 ps, respectively. Using the simplified efficiency expression $\Phi_{DA} = k_{DA}/(k_{DA} + k_{IC})$, where $k_{IC} = 0.0625\ ps^{-1}$ for $S_1 \rightarrow S_0$ internal conversion, we get maximum quantum efficiencies of 85.75 and 84.65%, respectively, for the $S_1 \rightarrow Q_y$ pathway. We note that both the PID612 and PID622 S_1 emission excited states also had the most observable ICT characteristics as shown in Figure 8. The $S_1 \rightarrow Q_x$ pathway does not compete with the $S_1 \rightarrow Q_y$ pathway, with the shortest lifetime of 554 from PID622 to CLA602. The $S_2 \rightarrow Q_x$ pathway, considered a relatively high yield pathway in PCP by many theorists and experimentalists, competes with the extremely fast $S_2 \rightarrow S_1$ internal conversion rate (estimated as $k_{IC} = 5-20\ ps^{-1}$). We conservatively use the value $k_{IC} = 5\ ps^{-1}$ in our quantum efficiency calculations, but the highest efficiency noted is 3.74% between PID613 and CLA601. Thus, the $S_2 \rightarrow Q_x$ pathway will occur in PCP but not at rates previously hypothesized (up to 25%); rather, it represents only a small contribution according to our calculations.[12,13] We do note that using the IDA for the $S_2 \rightarrow Q_x$ calculation greatly increases the perceived rate of EET, with one pathway (PID614 → CLA601) reaching almost 25% efficiency, but, as previously discussed, the dipole−dipole couplings are generally not a good approximation for the Coulombic couplings in the PCP complex. Unfortunately, our calculations cannot explain the fast chlorophyll *a* bleaching (<200) seen in experiments with an $S_2 \rightarrow Q_x$ energy transfer pathway. This is an issue that merits considerable future study, but it is certainly possible that the extremely strong excitonic coupling between peridinin S_2 excited states, which is discussed later, has an effect on the $S_2 \rightarrow Q_x$ pathway.

Since the $S_1 \rightarrow Q_y$ EET pathway is the dominant peridinin to chlorophyll *a* pathway, we estimate an average transfer rate of $1.44 \times 10^{-1}\ ps^{-1}$ and an average lifetime of 6.93 ps assuming that all eight peridinin to chlorophyll *a* pathways have an equal probability of occurrence. We suspect that this is not a valid assumption and that excitation energy is instead funneled to the dominant S_1 excited states (PID612 and PID622) before EET occurs between peridinin and chlorophyll *a*; this would lead to the lower average lifetime of 2.3−3.2 ps found in experimental studies of PCP.

While our V_{DA} interaction terms using the TDC approximation may be considered to be as accurate as the wave functions upon which they are based, our J_{DA} terms are calculated using a number of approximations due to the lack of experimental spectra, especially for the S_1 and Q_x excited states. Even so, we believe that we are in the correct order of magnitude with these values, and since k_{DA} correlates linearly with J_{DA}, we do not expect any significant change in EET rates and efficiencies based on the spectral overlap error.

Peridinin → Peridinin EET. In Table 5, we compare the Coulombic couplings, V_{DA}, and spectral overlap integrals, J_{DA}, for the two pathways of peridinin to peridinin EET studied in this paper: $S_1 \rightarrow S_1$ and $S_2 \rightarrow S_2$. Both $S_1 \rightarrow S_1$ and $S_2 \rightarrow S_2$ have significant Coulombic couplings, but the couplings between S_2 excited states are 1 to 2 orders of magnitude larger than those between S_1 excited states and are the largest couplings studied in this work by a significant margin. Again, we note that the Coulombic couplings calculated using the dipole−dipole interaction are not a good approximation for the full TDC interaction; this is especially true for the $S_2 \rightarrow S_2$ dipole−dipole couplings, which approach unrealistically large values. Spectral overlap terms for S_2 interactions are larger than those for S_1 interactions, which is not surprising given the extremely large apparent Stokes shift between S_1 absorption and emission energies due to the peak in the S_1 excited state occurring at the (0−2) vibronic band.

In Table 6, we compare the rates, lifetimes, and efficiencies of these pathways as calculated using EET in eq 1. Quantum efficiencies in this table are calculated using the following rates of internal conversion: $k_{IC} = 0.0625\ ps^{-1}$ for $S_1 \rightarrow S_0$ and $k_{IC} = 5\ ps^{-1}$ for $S_2 \rightarrow S_1$. The $S_1 \rightarrow S_1$ pathway is moderately efficient, with several efficiencies in the 40% range. Unfortunately, this pathway competes with the much more efficient $S_1 \rightarrow Q_y$ route

dx.doi.org/10.1021/jp5017054 | J. Phys. Chem. B 2014, 118, 9141−9154

of energy transfer to chlorophyll *a*. It is possible that this pathway is utilized to direct the excitation to a more successful energy donor (e.g., PID612 or PID622) if the S_1 excited state is trapped on a less successful energy donor (e.g., PID611 or PID623, both of whose calculated EET efficiencies to chlorophyll *a* are less than 5%). On the other hand, the $S_2 \rightarrow S_2$ pathway is extremely fast and efficient, with all calculated efficiencies above 70%, and many greater than 90%. It is important to note again that in Table 6 the IDA for the $S_2 \rightarrow S_2$ pathway results in artificially large rates that correspond to EET lifetimes of less than 1 fs. Also, the spectral overlap integrals are based on a number of approximations, but we do not expect the error inherent in the J_{DA} term to significantly affect our calculated EET rates and efficiencies.

The magnitude of the calculated Coulombic couplings suggests that the S_2 excited states are excitonically coupled in several dominant pairs (e.g., PID611 and PID612, PID613 and PID614),[7] and the exciton is transferred throughout the complex until the energy is transferred to the Q_x band via EET or, more likely, until the S_2 exciton relaxes to the S_1 state via internal conversion. We hypothesize that this may serve the purpose of funneling the excited state energy toward the more successful peridinin energy donors (e.g., the PID612 and PID622 S_1 states), similar to our suggestion above regarding the $S_1 \rightarrow S_1$ pathway. The properties of the hypothetical S_2 exciton pairs are outside the scope of this study since we have focused on single-molecule calculations, but they could be investigated in future work.

CONCLUSIONS

We developed a new method—integrating complete active space configuration interaction calculations to obtain excited state properties with the transition density cube method to calculate Coulombic couplings for the FRET model—to model excitation energy transfer in the peridinin-chlorophyll *a*-protein complex of *Amphidinium carterae*. The use of configuration interaction was necessitated by the significant double excitation character in the peridinin S_1 excited state. We employed the semiempirical MNDO method and an active space of six molecular orbitals for the CAS-CI calculations. We also wrote a Python script to calculate transition densities and create transition density cube files for the MOPAC 2012 software package. The transition density cube files generated using this methodology are accurate to within 0.05% of the original wave function(s), resulting in Coulombic couplings that are much more accurate than those calculated using the dipole−dipole approximation.

The excited state energies calculated for both peridinin and chlorophyll *a* match reasonably with available experimental data, but the shape/width of the spectral overlap integrals are still fitted to experimental data since the errors in excited state energy shifts are inconsistent between the different peridinin and chlorophyll *a* excited states. Peridinin excited states S_1 and S_2 are highly dependent upon the polyene chain geometry and local environment due to protein electrostatics, whereas chlorophyll *a* excited states Q_y and Q_x are very similar in CLA601 and CLA602. Nevertheless, the peridinin excited states are still similar in electronic structure, with most S_1 states consisting of around 60% double-excitation character and most S_2 states consisting of nearly 90% single-excitation character. We notice some intramolecular charge transfer character in a few of the peridinin S_1 excited states, and this characteristic is dependent on the pigment geometry and local environment. Since we do not see a separate ICT excited state as suggested in some previous studies, we hypothesize that this is instead a characteristic of the S_1 state; thus, it is dependent on the structural configuration of the pigments and dictates the energy transfer efficiency within the complex. We observed that the peridinin S_1 emission excited states with significant ICT characteristics (e.g., PID612 and PID622) also contributed to the fastest $S_1 \rightarrow Q_y$ pathways in the PCP complex.

The calculated Coulombic couplings in Tables 3 and 5, using both the dipole−dipole approximation and the transition density cube method, prove that the dipole−dipole approximation cannot adequately approximate the full Coulombic coupling for the interactions in the PCP complex between peridinin and chlorophyll *a* and between two peridinin molecules. This finding is not surprising due to the close proximity of the pigments in PCP. In our calculations, the $S_1 \rightarrow Q_y$ pathway was the dominant mode of EET between peridinin and chlorophyll *a* molecules in PCP, with the PID612 to CLA601 and PID622 to CLA602 pathways being the most efficient; they have lifetimes of 2.66 ps and 2.90 ps and efficiencies of 85.75 and 84.65%, respectively. We do not see any significant energy transfer using the $S_1 \rightarrow Q_x$ or $S_2 \rightarrow Q_x$ pathways that were suggested by other researchers, and we cannot presently explain the fast chlorophyll *a* bleaching (<200 fs) seen in experiments.

The calculated Coulombic couplings for the $S_2 \rightarrow S_2$ energy transfer pathway are extremely large, which suggests either excitonic coupling between pairs of peridinin S_2 excited states and/or extremely fast energy transfer between S_2 states on the order of roughly 10−60 fs; these would compete favorably with the extremely fast $S_2 \rightarrow S_1$ internal conversion rate of $k_{IC} = 5-20\ ps^{-1}$. The calculated $S_1 \rightarrow S_1$ energy transfer pathway shows moderate efficiency (4−45%) but cannot compete with the relatively fast $S_1 \rightarrow Q_y$ EET pathway. We hypothesize that the peridinin to peridinin energy transfer pathways enhance the energy transfer efficiency by funneling the excited state energy toward the most successful S_1 excited states (e.g., PID612 and PID622). This hypothesis, along with the dependence of the S_1/ICT excited state on pigment and protein structure, may be studied as the subject of future work using an all-atom QM/MM simulation so that a larger sampling of structural degrees of freedom could be included.

AUTHOR INFORMATION

Corresponding Author

*E-mail: clo@wustl.edu

Notes

The authors declare no competing financial interest.

ACKNOWLEDGMENTS

We thank Sergei Tretiak and Christopher Duffy for useful discussions relating to excitation energy transfer, Brent Krueger for assistance with the TDC code, and James Stewart for assistance with the MOPAC code. This material was based on work supported as part of the Photosynthetic Antenna Research Center (PARC), an Energy Frontier Research Center funded by the U.S. Department of Energy, Office of Science, Office of Basic Energy Sciences under award number DE-SC 0001035. This work was also performed, in part, at the Center for Integrated Nanotechnologies, an Office of Science User Facility operated for the U.S. Department of Energy (DOE) Office of Science by Los Alamos National Laboratory (contract

DE-AC52-06NA25396) and Sandia National Laboratories (contract DE-AC04-94AL85000).

REFERENCES

(1) Blankenship, R. E. *Molecular Mechanisms of Photosynthesis*; Blackwell Publishing: Williston, VT, 2002.

(2) Blankenship, R. E.; Tiede, D. M.; Barber, J.; Brudvig, G. W.; Fleming, G.; Ghirardi, M.; Gunner, M. R.; Junge, W.; Kramer, D. M.; Melis, A.; et al. Comparing Photosynthetic and Photovoltaic Efficiencies and Recognizing the Potential for Improvement. *Science* **2011**, *332*, 805−809.

(3) Hofmann, E.; Wrench, P. M.; Sharples, F. P.; Hiller, R. G.; Welte, W.; Diederichs, K. Structural Basis of Light Harvesting by Carotenoids: Peridinin-Chlorophyll-Protein from *Amphidinium carterae*. *Science* **1996**, *272*, 1788−1791.

(4) Berman, H. M.; Westbrook, J.; Feng, Z.; Gilliland, G.; Bhat, T. N.; Weissig, H.; Shindyalov, I. N.; Bourne, P. E. The Protein Data Bank. *Nucleic Acids Res.* **2000**, *28*, 235−242.

(5) Humphrey, W.; Dalke, A.; Schulten, K. VMD: Visual Molecular Dynamics. *J. Mol. Graphics* **1996**, *14*, 33−38.

(6) Stone, J. An Efficient Library for Parallel Ray Tracing and Animation. M.Sc. Thesis, Computer Science Department, University of Missouri—Rolla, 1998.

(7) Damjanovic′, A.; Ritz, T.; Schulten, K. Excitation Transfer in the Peridinin-Chlorophyll-Protein of *Amphidinium carterae*. *Biophys. J.* **2000**, *79*, 1695−1705.

(8) Bautista, J. A.; Hiller, R. G.; Sharples, F. P.; Gosztola, D.; Wasielewski, M.; Frank, H. A. Singlet and Triplet Energy Transfer in the Peridinin-Chlorophyll *a* Protein from *Amphidinium carterae*. *J. Phys. Chem. A* **1999**, *103*, 2267−2273.

(9) Akimoto, S.; Takaichi, S.; Ogata, T.; Nishimura, Y.; Yamazaki, I.; Mimuro, M. Excitation Energy Transfer in Carotenoid-Chlorophyll Protein Complexes Probed by Femtosecond Fluorescence Decays. *Chem. Phys. Lett.* **1996**, *260*, 147−152.

(10) Jiang, J.; Zhang, H.; Kang, Y.; Bina, D.; Lo, C. S.; Blankenship, R. E. Characterization of the Peridinin-Chlorophyll *a*-Protein Complex in the Dinoflagellate *Symbiodinium*. *Biochim. Biophys. Acta, Bioenerg.* **2012**, *1817*, 983−989.

(11) Bautista, J. A.; Connors, R. E.; Raju, B. B.; Hiller, R. G.; Sharples, F. P.; Gosztola, D.; Wasielewski, M. R.; Frank, H. A. Excited State Properties of Peridinin: Observation of a Solvent Dependence of the Lowest Excited Singlet State Lifetime and Spectral Behavior Unique among Carotenoids. *J. Phys. Chem. B* **1999**, *103*, 8751−8758.

(12) Krueger, B. P.; Lampoura, S. S.; van Stokkum, I. H. M.; Papagiannakis, E.; Salverda, J. M.; Gradinaru, C. C.; Rutkauskas, D.; Hiller, R. G.; van Grondelle, R. Energy Transfer in the Peridinin-Chlorophyll *a*-Protein of *Amphidinium carterae* Studied by Polarized Transient Absorption and Target Analysis. *Biophys. J.* **2001**, *80*, 2843−2855.

(13) Zigmantas, D.; Hiller, R. G.; Sundström, V.; Polívka, T. Carotenoid to Chlorophyll Energy Transfer in the Peridinin-Chlorophyll *a*-Protein Complex Involves an Intramolecular Charge Transfer State. *Proc. Natl. Acad. Sci. U.S.A.* **2002**, *99*, 16760−16765.

(14) Zigmantas, D.; Polívka, T.; Hiller, R. G.; Yartsev, A.; Sundström, V. Spectroscopic and Dynamic Properties of the Peridinin Lowest Singlet Excited States. *J. Phys. Chem. A* **2001**, *105*, 10296−10306.

(15) Niedzwiedzki, D. M.; Chatterjee, N.; Enriquez, M. M.; Kajikawa, T.; Hasegawa, S.; Katsumura, S.; Frank, H. A. Spectroscopic Investigation of Peridinin Analogues Having Different π-Electron Conjugated Chain Lengths: Exploring the Nature of the Intramolecular Charge Transfer State. *J. Phys. Chem. B* **2009**, *113*, 13604−13612.

(16) Zigmantas, D.; Hiller, R. G.; Yartsev, A.; Sundström, V.; Polívka, T. Dynamics of Excited States of the Carotenoid Peridinin in Polar Solvents: Dependence on Excitation Wavelength, Viscosity, and Temperature. *J. Phys. Chem. B* **2003**, *107*, 5339−5348.

(17) Linden, P. A.; Zimmermann, J.; Brixner, T.; Holt, N. E.; Vaswani, H. M.; Hiller, R. G.; Fleming, G. R. Transient Absorption Study of Peridinin and Peridinin-Chlorophyll *a*-Protein after Two-Photon Excitation. *J. Phys. Chem. B* **2004**, *108*, 10340−10345.

(18) Chatterjee, N.; Niedzwiedzki, D. M.; Kajikawa, T.; Hasegawa, S.; Katsumura, S.; Frank, H. A. Effect of π-Electron Conjugation Length on the Solvent-Dependent S_1 Lifetime of Peridinin. *Chem. Phys. Lett.* **2008**, *463*, 219−224.

(19) Chatterjee, N.; Niedzwiedzki, D. M.; Aoki, K.; Kajikawa, T.; Katsumura, S.; Hashimoto, H.; Frank, H. A. Effect of Structural Modifications on the Spectroscopic Properties and Dynamics of the Excited States of Peridinin. *Arch. Biochem. Biophys.* **2009**, *483*, 146−155.

(20) Enriquez, M. M.; Hananoki, S.; Hasegawa, S.; Kajikawa, T.; Katsumura, S.; Wagner, N. L.; Birge, R. R.; Frank, H. A. Effect of Molecular Symmetry on the Spectra and Dynamics of the Intramolecular Charge Transfer (ICT) State of Peridinin. *J. Phys. Chem. B* **2012**, *116*, 10748−10756.

(21) Wagner, N. L.; Greco, J. A.; Enriquez, M. M.; Frank, H. A.; Birge, R. R. The Nature of the Intramolecular Charge Transfer State in Peridinin. *Biophys. J.* **2013**, *104*, 1314−1325.

(22) Kleima, F. J.; Hofmann, E.; Gobets, B.; van Stokkum, I. H. M.; van Grondelle, R.; Diederichs, K.; van Amerongen, H. Förster Excitation Energy Transfer in Peridinin-Chlorophyll-*a*-Protein. *Biophys. J.* **2000**, *78*, 344−353.

(23) Polívka, T.; Pascher, T.; Sundström, V.; Hiller, R. G. Tuning Energy Transfer in the Peridinin-Chlorophyll Complex by Reconstitution with Different Chlorophylls. *Photosynth. Res.* **2005**, *86*, 217−227.

(24) Carbonera, D.; Giacometti, G.; Segre, U.; Hofmann, E.; Hiller, R. G. Structure-Based Calculations of the Optical Spectra of the Light-Harvesting Peridinin-Chlorophyll-Protein Complexes from *Amphidinium carterae* and *Heterocapsa pygmaea*. *J. Phys. Chem. B* **1999**, *103*, 6349−6356.

(25) Scholes, G. D. Long-Range Resonance Energy Transfer in Molecular Systems. *Annu. Rev. Phys. Chem.* **2003**, *54*, 57−87.

(26) Engel, G. S.; Calhoun, T. R.; Read, E. L.; Ahn, T.-K.; Mančal, T.; Cheng, Y.-C.; Blankenship, R. E.; Fleming, G. R. Evidence for Wavelike Energy Transfer Through Quantum Coherence in Photosynthetic Systems. *Nature* **2007**, *446*, 782−786.

(27) Ishizaki, A.; Calhoun, T. R.; Schlau-Cohen, G. S.; Fleming, G. R. Quantum Coherence and its Interplay with Protein Environments in Photosynthetic Electronic Energy Transfer. *Phys. Chem. Chem. Phys.* **2010**, *12*, 7319−7337.

(28) Scholes, G. D.; Fleming, G. R.; Olaya-Castro, A.; van Grondelle, R. Lessons from Nature about Solar Light Harvesting. *Nat. Chem.* **2012**, *3*, 763−774.

(29) Fermi, E. *Nuclear Physics*; University of Chicago Press: Chicago, IL, 1950.

(30) Duffy, C. D. P.; Valkunas, L.; Ruban, A. V. Quantum Mechanical Calculations of Xanthophyll-Chlorophyll Electronic Coupling in the Light-Harvesting Antenna of Photosystem II of Higher Plants. *J. Phys. Chem. B* **2013**, *117*, 7605−7614.

(31) Förster, T. Zwischenmolekulare Energiewanderung und Fluoreszenz. *Ann. Phys.* **1948**, *437*, 55−75.

(32) Förster, T. 10th Spiers Memorial Lecture: Transfer Mechanisms of Electronic Excitation. *Discuss. Faraday Soc.* **1959**, *27*, 7−17.

(33) Debreczeny, M. P.; Wasielewski, M. R.; Shinoda, S.; Osuka, A. Singlet-Singlet Energy Transfer Mechanisms in Covalently-Linked Fucoxanthin- and Zeaxanthin-Pyropheophorbide Molecules. *J. Am. Chem. Soc.* **1997**, *119*, 6407−6414.

(34) Sener, M.; Strümpfer, J.; Hsin, J.; Chandler, D.; Scheuring, S.; Hunter, C. N.; Schulten, K. Förster Energy Transfer Theory as Reflected in the Structures of Photosynthetic Light-Harvesting Systems. *ChemPhysChem* **2011**, *12*, 518−531.

(35) Krueger, B. P.; Scholes, G. D.; Fleming, G. R. Calculation of Couplings and Energy-Transfer Pathways between the Pigments of LH2 by the *ab initio* Transition Density Cube Method. *J. Phys. Chem. B* **1998**, *102*, 5378−5386.

(36) Krueger, B. *The Transition Density Cube Method*; The Krueger Laboratory for Biophysics Research at Hope College: Holland, MI, 2005; www.chem.hope.edu/~krieg/TDC/TDC_home.htm.
(37) Di Valentin, M.; Tait, C. E.; Salvadori, E.; Orian, L.; Polimeno, A.; Carbonera, D. Evidence for Water-Mediated Triplet-Triplet Energy Transfer in the Photoprotective Site of the Peridinin-Chlorophyll *a*-Protein. *Biochim. Biophys. Acta* **2014**, *1837*, 85−97.
(38) *Suite 2009: Maestro*, version 9.0; Schrödinger: New York, 2009.
(39) Stewart, J. J. P. Application of Localized Molecular Orbitals to the Solution of Semiempirical Self-Consistent Field Equations. *Int. J. Quantum Chem.* **1996**, *58*, 133−146.
(40) Stewart, J. J. P. Calculation of the Geometry of a Small Protein using Semiempirical Self-Consistent Field Equations. *J. Mol. Struct.: THEOCHEM* **1997**, 195−205.
(41) Stewart, J. J. P. *MOPAC2012*; Stewart Computational Chemistry: Colorado Springs, CO, 2012; http://openmopac.net.
(42) Dewar, M. J. S.; Thiel, W. Ground States of Molecules. 38. The MNDO method. Approximations and Parameters. *J. Am. Chem. Soc.* **1977**, *99*, 4899−4907.
(43) Stewart, J. J. P. Optimization of Parameters for Semiempirical Methods IV: Extension of MNDO, AM1, and PM3 to More Main Group Elements. *J. Mol. Model.* **2004**, *10*, 155−164.
(44) Mulliken, R. S. Electronic Population Analysis on LCAO-MO Molecular Wave Functions. *J. Chem. Phys.* **1955**, *23*, 1833−1841.
(45) Kohn, W.; Sham, L. J. Self-Consistent Equations Including Exchange and Correlation Effects. *Phys. Rev.* **1965**, *140*, A1133−A1138.
(46) Runge, E.; Gross, E. K. U. Density-Functional Theory for Time-Dependent Systems. *Phys. Rev. Lett.* **1984**, *52*, 997−1000.
(47) Vaswani, H. M.; Hsu, C.-P.; Head-Gordon, M.; Fleming, G. R. Quantum Chemical Evidence for an Intramolecular Charge-Transfer State in the Carotenoid Peridinin of Peridinin-Chlorophyll-Protein. *J. Phys. Chem. B* **2003**, *107*, 7940−7946.
(48) Schulten, K.; Karplus, M. On the Origin of a Low-Lying Forbidden Transition in Polyenes and Related Molecules. *Chem. Phys. Lett.* **1972**, *14*, 305−309.
(49) Tavan, P.; Schulten, K. The Low-Lying Electronic Excitations in Long Polyenes: A PPP-MRD-CI Study. *J. Chem. Phys.* **1986**, *85*, 6602−6609.
(50) Shavitt, I. *Modern Theoretical Chemistry*; Plenum Press: New York, 1976.
(51) Szalay, P. G.; Müller, T.; Gidofalvi, G.; Lischka, H.; Shepard, R. Multiconfiguration Self-Consistent Field and Multireference Configuration Interaction Methods and Applications. *Chem. Rev.* **2012**, *112*, 108−181.
(52) Knecht, S.; Marian, C. M.; Kongsted, J.; Mennucci, B. On the Photophysics of Carotenoids: A Multireference DFT Study of Peridinin. *J. Phys. Chem. B* **2013**, *117*, 13808−13815.
(53) Macernis, M.; Sulskus, J.; Duffy, C. D. P.; Ruban, A. V.; Valkunas, L. Electronic Spectra of Structurally Deformed Lutein. *J. Phys. Chem. A* **2012**, *116*, 9843−9853.
(54) Warshel, A.; Sharma, P. K.; Kato, M.; Parson, W. W. Modeling Electrostatic Effects in Proteins. *Biochim. Biophys. Acta* **2006**, *1764*, 1647−1676.
(55) Szabo, A.; Ostlund, N. S. *Modern Quantum Chemistry: Introduction to Advanced Electronic Structure Theory*; McGraw-Hill: New York, 1989.
(56) Stewart, J. J. P. Optimization of Parameters for Semiempirical Methods V: Modification of NDDO Approximations and Application to 70 Elements. *J. Mol. Model.* **2007**, *13*, 1173−1213.
(57) Christensen, R. L.; Goyette, M.; Gallagher, L.; Duncan, J.; DeCoster, B.; Lugtenburg, J.; Jansen, F. J.; van der Hoef, I. S_2 and S_2 States of Apo- and Diapocarotenes. *J. Phys. Chem. A* **1999**, *103*, 2399−2407.
(58) Zimmermann, J.; Linden, P. A.; Vaswani, H. M.; Hiller, R. G.; Fleming, G. R. Two-Photon Excitation Study of Peridinin in Benzene and in the Peridinin Chlorophyll *a*-Protein (PCP). *J. Phys. Chem. B* **2002**, *106*, 9418−9423.
(59) Shima, S.; Ilagan, R. P.; Gillespie, N.; Sommer, B. J.; Hiller, R. G.; Sharples, F. P.; Frank, H. A.; Birge, R. R. Two-Photon and Fluorescence Spectroscopy and the Effect of Environment on the Photochemical Properties of Peridinin in Solution and in the Peridinin-Chlorophyll-Protein from *Amphidinium carterae*. *J. Phys. Chem. A* **2003**, *107*, 8052−8066.
(60) Ditchfield, R.; Hehre, W. J.; Pople, J. A. Self-Consistent Molecular-Orbital Methods. IX. An Extended Gaussian-Type Basis for Molecular-Orbital Studies of Organic Molecules. *J. Chem. Phys.* **1971**, *54*, 724−728.
(61) Hehre, W. J.; Ditchfield, R.; Pople, J. A. Self-Consistent Molecular Orbital Methods. XII. Further Extensions of Gaussian-Type Basis Sets for Use in Molecular Orbital Studies of Organic Molecules. *J. Chem. Phys.* **1972**, *56*, 2257−2261.
(62) Hariharan, P. C.; Pople, J. A. The Influence of Polarization Functions on Molecular Orbital Hydrogenation Energies. *Theor. Chem. Acc.* **1973**, *28*, 213−222.
(63) Becke, A. D. Density-Functional Thermochemistry. III. The Role of Exact Exchange. *J. Chem. Phys.* **1993**, *98*, 5648−5652.
(64) Frisch, M. J.; Trucks, G. W.; Schlegel, H. B.; Scuseria, G. E.; Robb, M. A.; Cheeseman, J. R.; Scalmani, G.; Barone, V.; Mennucci, B.; Petersson, G. A. et al. *Gaussian 09*, Revision A.02; Gaussian Inc.: Wallingford, CT, 2009.
(65) Kleima, F. J.; Wendling, M.; Hofmann, E.; Peterman, E. J. G.; van Grondelle, R.; van Amerongen, H. Peridinin-Chlorophyll *a*-Protein: Relating Structure and Steady-State Spectroscopy. *Biochemistry* **2000**, *39*, 5184−5195.
(66) Gouterman, M. Spectra of Porphyrins. *J. Mol. Spectrosc.* **1961**, *6*, 138−163.
(67) Gouterman, M.; Wagniere, G. H. Spectra of Porphyrins. Part II. Four Orbital Model. *J. Mol. Spectrosc.* **1963**, *11*, 108−127.